#### RESEARCH ARTICLE



# 3-Dimensional CFD Simulation of Pre-Wastewater Treatment via Multi-Channel Porous Ceramic Membrane

Sina Fazlifard\*, Seyed Sepehr Mostafayi, and Taha Baghban Ronaghi

## ABSTRACT

Multi-channel microfiltration (MF) membranes are considered as one of the most efficient separation methods for wastewater treatment, mainly due to their relatively high thermal and chemical resistance. Among various types of MF membranes, Ceramic Membranes attract great attention because of their high active area and superb mechanical strength, making them an industrially applicable pretreatment process for Reverse Osmosis (RO) unit operation. Here, a thorough 3-dimensional modeling of a 19-channel Ceramic Membrane was employed in order to gain insight into pressure drop, velocity distribution, and concentration profile in each channel. Experimental data from a lab-scale multi-channel Ceramic Membrane fed with oily wastewater was used to validate the model. The permeate flux was predicted as 200 to 250 L/m<sup>2</sup>.hr based on the porous media transmission pressure in such configurations. Further, permeate mass flux was also calculated based on the inlet flow velocities ranging from 0.75 to 2.25 m/s.

Keywords: Ceramic Membrane, CFD, Multi-channel, Wastewater treatment.

Submitted: December 01, 2023 Published: March 02, 2024

10.24018/ejeng.2024.9.1.3128

Illinois Institute of Technology, USA.

\*Corresponding Author: e-mail: sfazlifard@hawk.iit.edu

#### 1. Introduction

Nowadays, finding a suitable wastewater treatment method has become a priority worldwide, mainly because of its impact on human health and the sustainability of the environment [1], [2]. Membrane processes have increasingly become applicable for water production in different industries [3]. Besides that, this method is helpful in various industries to separate wastewater polluted with organic components [4]. One of the efficient methods for wastewater treatment is membrane processes. In addition to maintaining the cleanliness of the water supplies, this technique uses less energy and emits less greenhouse gases [5]. Because of their excellent mechanical, thermal, and chemical resistance, ceramic membranes are one of the intriguing types of membranes applicable to producing high-quality water [6]. Ceramic membranes have various shapes, including disk, tubular, multi-channel, and hollow fiber membranes. Multi-channel ceramic membranes have attracted the most attention among all these structures because of their high active area and mechanical strength [7]. One of the possible applications of this type could be a pretreatment step before reverse osmosis (RO), the most popular method for making drinking water from seawater [8].

Researchers have worked in recent years to improve wastewater treatment utilizing ceramic membranes. Computational Fluid Dynamics (CFD) is a valuable technique for investigating this process, which facilitates understanding the membrane process's mechanism by providing novel models and data [9]. With this highly valuable method that facilitates understanding the system's details on the microscopic scale, some researchers have studied various membrane systems in different conditions. Frederic et al. [10] modeled three types of multi-channel ceramic membranes with different geometry, including 31 circular channels, 8 square channels, and 64 square channels. A 2dimensional model has been used to study fluid flow and fouling distribution profile as a result of filtered volume. They investigated the fouling of selective layers that may affect the flow profile inside the channels of multi-channel ceramic membranes. They combined the Darcy flow model with a resistance-in-series model in the cross sections of membranes as a 2-dimensional geometry. Zare et al. [11] developed a 2-dimensional finite volume model for CFD

modeling of laminar flow in a cross-flow micro-filter membrane with a narrow rectangular channel. To increase the accuracy, they used the Eulerian multiphase model for multiphase flow equations. They used local pressure distribution to calculate the permeation flux and determine the concentration polarization profile. Neto et al. [9] studied the effect of different process variables on the performance of a ceramic membrane separation system using CFD modeling. The authors reported that the feed flow rate has a high impact on trans-membrane pressure; however, the increase in the ceramic membrane's porosity did not significantly influence the system's performance. Tong et al. [12] used CFD modeling of a 19-core ceramic membrane to investigate the flow rate's effect on the membrane module's resistance. The authors reported that with an increase in the flow rate from 26 to 89 m<sup>3</sup>/h, the resistance of the membrane system grows continuously.

The 3-dimensional CFD simulation of wastewater treatment using a 19-channel ceramic membrane is presented in this work. Most research on multi-channel membrane research used 2-dimensional models of a single channel. Because each channel has a different pressure drop and concentration distribution, each channel has a different mass fluxes and efficiency level. In order to address the issue, our work builds a 3-dimensional model of the complete system.

#### 2. Materials and Methods

## 2.1. Experimental Data

The structural characteristics of the ceramic membrane used for wastewater treatment are presented in Table I. Abadi et al. [13] used a multi-channel membrane to separate wastewater, and the model of this paper is validated using that data. The isothermal and steady-state approaches are assumed for this simulation. The components' physical and chemical properties are also constant, and the flow regime is laminar. The research membrane module consists of channels through which the wastewater flows and a porous media through which the permeate flow, purified water, diffuses.

TABLE I: MEMBRANE AND OPERATIONAL

Properties [13]					
Items	Symbol	Amount			
Channel	$r_1$	4 mm			
diameter					
Module	$r_2$	30 mm			
diameter					
Module length	L	1033 cm			
Number of	N	19			
channels					
Porosity	$\varepsilon$	0.44%			
Distance	_	1.5–2 mm			
between					
channels					
Temperature	T	298 K			

## 2.2. Porous Media Equations and Boundary Conditions

The continuity equation for each component is provided in (1):

$$\frac{\partial C_i}{\partial t} = -\left(\nabla . C_i V\right) - \left(\nabla . J_i\right) + R_i \tag{1}$$

where V,  $J_i$ ,  $R_i$ ,  $C_i$ , and t are velocity, diffusion flux, reaction rate, component concentration, and time, respectively.

The reaction rate between components and the porous media is negligible. Therefore,  $R_i$  is assumed to be zero, and (2) can be used for each component as the continuity equation in the cylindrical coordinates in the porous media:

$$D_{i-shell} \left[ \frac{\partial^{2} C_{i-porous \, media}}{\partial r^{2}} + \frac{1}{r} \frac{\partial C_{i-porous \, media}}{\partial r} \right]$$

$$+ \frac{\partial^{2} C_{i-porous \, media}}{\partial z^{2}}$$

$$= V_{z-porous \, media} \frac{\partial C_{i-porous \, media}}{\partial z}$$
(2)

On the other hand, in the porous media, the bulk velocity does not exist; consequently, the diffusion equation can be expressed as (3):

$$D_{i-porous\,media} \left[ \frac{\partial^{2} C_{i-porous\,media}}{\partial r^{2}} + \frac{1}{r} \frac{\partial C_{i-porous\,media}}{\partial r} + \frac{\partial^{2} C_{i-porous\,media}}{\partial z^{2}} \right] = 0$$
(3)

The boundary conditions are as (4)–(7):

$$at z = 0, \quad \frac{\partial C_{i-porous media}}{\partial z} = 0$$
 (4)

$$at r = r_1, \quad C_{i-porous media} = C_{i-channel}$$
 (5)

$$at r = r_2, \quad \frac{\partial C_{i-porous media}}{\partial r} = 0$$
 (6)

$$at z = L, \quad P = P_{atm}$$
 (7)

## 2.3. Channels Equations and Boundary Conditions

In the steady-state condition, the transfer equation to transport from feed to porous media is given in (8) for each component:

$$D_{i-channel} \left[ \frac{\partial^{2} C_{i-channel}}{\partial r^{2}} + \frac{1}{r} \frac{\partial C_{i-channel}}{\partial r} + \frac{\partial^{2} C_{i-channel}}{\partial z^{2}} \right]$$

$$= V_{z-channel} \frac{\partial C_{i-channel}}{\partial z}$$
(8)

The velocity profile in channels can be achieved from the Navier-Stokes equation given in (9):

$$\rho \frac{\partial V}{\partial t} - \mu \nabla V + \rho (V.\nabla) V + \nabla p = 0; \nabla V. V = 0$$
 (9)

where V is the velocity in the channels.

The boundary conditions are as (10)–(13):

$$at z = 0, \quad C_{i-channel} = C_{i0} \tag{10}$$

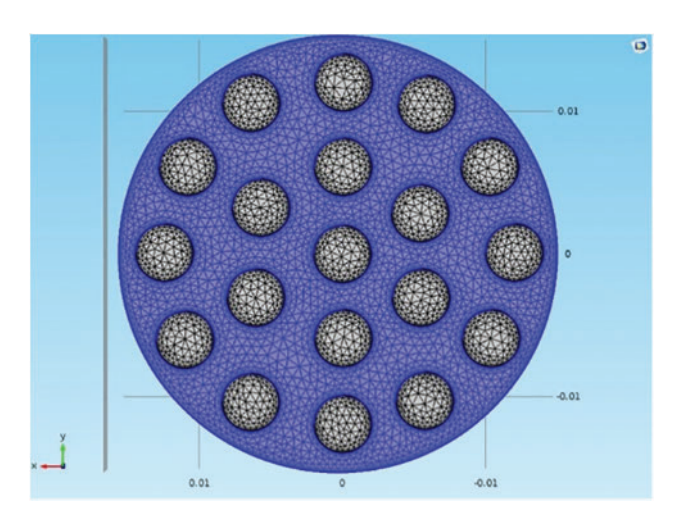


Fig. 1. System's geometry and meshing.

$$at r = r_1, \quad C_{i-channel} = C_{i-porous media}$$
 (11)

$$at z = L, \quad P = P_{atm}$$
 (12)

$$at r = 0, \quad \frac{\partial C_{i-channel}}{\partial r} = 0$$
 (13)

The removal percentage for each pollutant can be calculated by (14):

$$\%Removal = \frac{V_{in}C_{i_{in}} - V_{out}C_{i_{out}}}{V_{in}C_{i_{in}}} \times 100$$
 (14)

where  $C_{out}$  and  $C_{in}$  are the pollutant concentrations in the enter and exit.  $V_{out}$  and  $V_{in}$  are the volume flow of exit and enter, respectively.

C<sub>i</sub> out can be measured by (15) in the exit of porous media:

$$C_{iout} = \frac{\int C_i(r) dA}{\int dA},$$
 (15)

where A is wastewater exit area, Z = 0, and  $V_{out}$  can be determined from the volume balance of enter wastewater with all exits from porous media and all channels.

## 2.4. Solution

The governing equations and boundary conditions are coupled and solved together, in which the base of the solution are common parameters and equal boundary conditions in the interfaces. Using adaptive meshing, the largest meshing element is 1/100 to the system's smallest dimension. Furthermore, with this method, the meshing is concentrated the elements into the zones with large gradients, such as boundary layers. In Fig. 1, the crosssectional view of the created geometry and the meshing scheme of the system is given.

## 3. RESULTS AND DISCUSSION

#### 3.1. Validation Study

The results are compared to the experimental results from Abadi et al. [13] to verify the developed model.

TABLE II: EXPERIMENT AND SIMULATION RESULTS COMPARISON

Content	Unit	Feed	Permeate experimental	Permeate simulation
Oil and grease content	mg/l	26	4.6	4
Total organic carbon (TOC)	mg/l	141	7.5	7
Turbidity	mg/l	21	0.33	0.3

The boundary and operational conditions are consistent with the mentioned experimental study. The comparison of results is indicated in the Table II. The validation study is based on comparing the concentration of pollutants in the post-processed water. As can be seen, the results from the model are almost consistent with the experimental results (around 7%–15% error).

## 3.2. Water Distribution Along the Membrane

Effluent enters the membrane channels with a pure water concentration of 0.72 kg/m<sup>3</sup>. Since the porous media is selective towards water molecules, water molecules will penetrate the porous media more and faster than impurities. Therefore, the water penetrating the porous media can be collected and considered permeating flow. It is known that during this process, the concentration of water in the feed decreases, which is shown in Fig. 2. In Fig. 2a, the effluent has entered the system, and the amount of pure water in the effluent is equal to its initial value (0.72 kg/m<sup>3</sup>). However, as shown in Fig. 2b, the mass of water in the retentate flow at the channels' exit has decreased. This reduction in water mass will be seen as a decrease in the feed flux coming out of the channels. Fig. 2c also shows how the mass concentration of water in the feed changes along a selected channel. All these results also remind us that the mass transfer rate of all channels to the porous media is different.

#### 3.3. Water Distribution in Porous Media

Fig. 3 shows the mass concentration distribution of water inside the porous media. Two sections of the model corresponding to the beginning (Fig. 3) and the end of the process (Fig. 3b) are given below to determine the effect of radial penetration along the membrane length. In Fig. 3a, due to insufficient time for penetration at the moment of feed entry, penetration into the porous medium has not taken place. Whereas in Fig. 3b, the penetration of water into the porous media is quite clear. It is assumed that the water reaches the outer radius of the model after radial penetration and is immediately collected from there. In such a way that there is no mass of water on the outer surface of the porous media, and this is evident from the distribution of mass concentration of water in the mentioned forms. Industrially, in order to realize this assumption, there is a shell usually made of stainless steel or polymer, which directs the mass flux of water coming out of the porous medium immediately outside so that the water concentration gradient is established on the sides of the porous media in order to maintain the mass transfer.

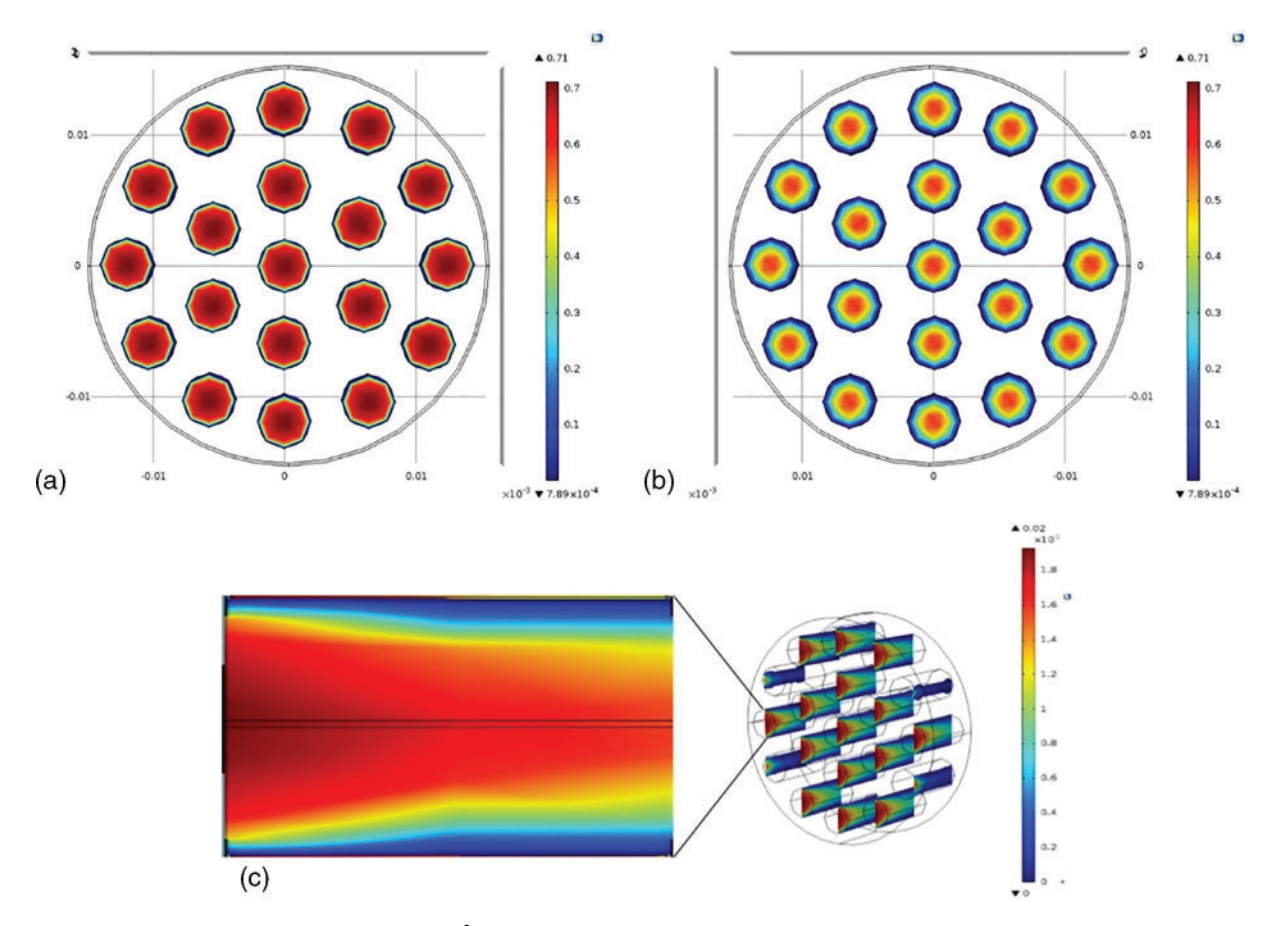


Fig. 2. Distribution of water concentration (kg/m<sup>3</sup>) of flow: (a) at the entrance of channels, (b) at the exit of channels, (c) along the channels.

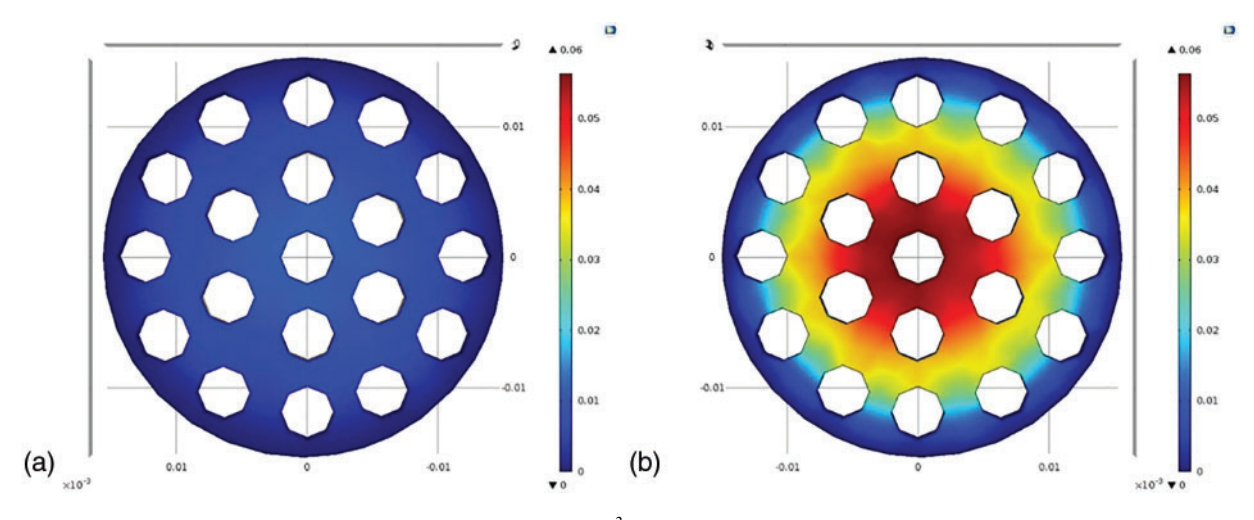


Fig. 3. Distribution of water concentration (kg/m<sup>3</sup>) in porous media: (a) at the entrance, (b) at the exit.

In Fig. 3b, the progress of water in the porous media to the outer side of the porous media is quite clear.

## 3.4. Pressure and Velocity Distribution

According to the assumptions, the channels' velocity is a laminar flow regime. Fig. 4 shows the velocity distribution inside the channels as a 2-dimensional graphical cut. As shown, the velocity is high at the beginning and in the entry section, but the velocity value is reduced in the exit section. This decrease is caused by the reduction of the mass passing through the channel due to penetration into the porous media, which, according to the continuity equation, causes a decrease in the flow velocity. On the other hand, the amount of penetration from different channels into the porous media is not the same. As a result, the velocity distribution in different channels will also be different. It is considered that the mechanism is only molecular penetration in the porous media. Thus, there will be no bulk mass transfer in this part.

Fig. 5 shows the 2-dimensional cut of how the pressure is distributed inside the channels at unit velocity. The feed enters the channels with a pressure higher than the atmospheric, and it is discharged to the atmospheric pressure environment, so the relative pressure of flow is considered zero.

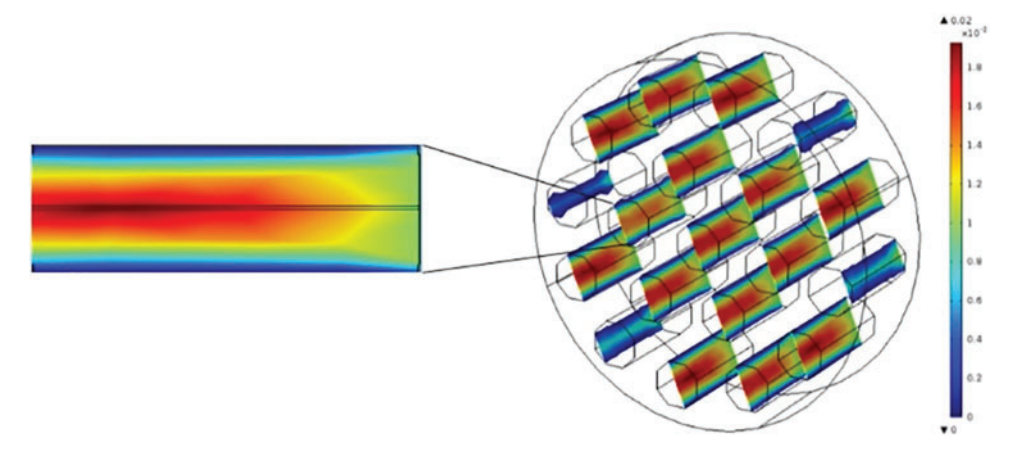


Fig. 4. Velocity distribution inside the channels (m/s).

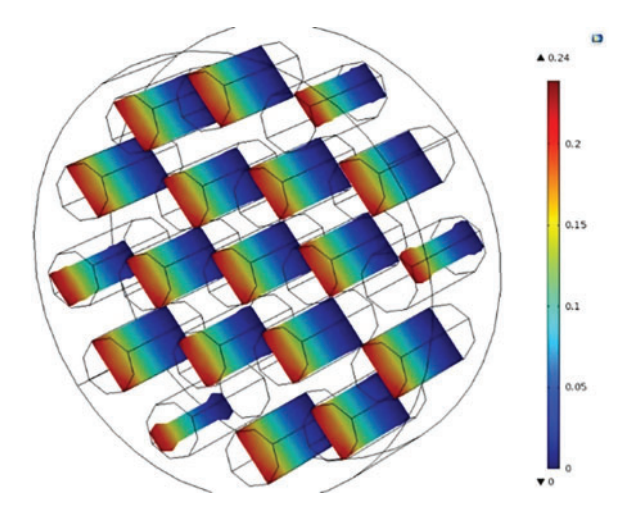


Fig. 5. Pressure distribution inside the channels at the unit velocity.

#### 3.5. Permeate Flux

Mass continuity is used to calculate the amount of water permeation flux from the porous media. In this way, the amount of exit flux from the channels can be calculated by the surface integration operation using the software. On the other hand, considering that the enter flux of the feed is also known, the difference between these two values is equal to the amount of flux penetrating the porous media, which is collected as purified water. The amount of volumetric and mass flux will be a constant value in a steady-state condition. Therefore, checking the mass flux value of purified water becomes meaningful in conditions where the operating conditions are variable, and the effect of those conditions on the process of change in purified water is investigated. In this regard, the effect of porous media transmission pressure (TMP) on the flux of purified water is investigated, the results of which are shown in Fig. 6. Although there is no bulk mass movement in the porous media, it should be noted that the pressure gradient is one of the driving forces of mass transfer. Therefore, the increase in transmission pressure difference has increased the permeate flux (purified water). Increasing the pressure parameter more than a certain amount does not affect the flux, which can be affected by the saturation of the porous blocking pores.

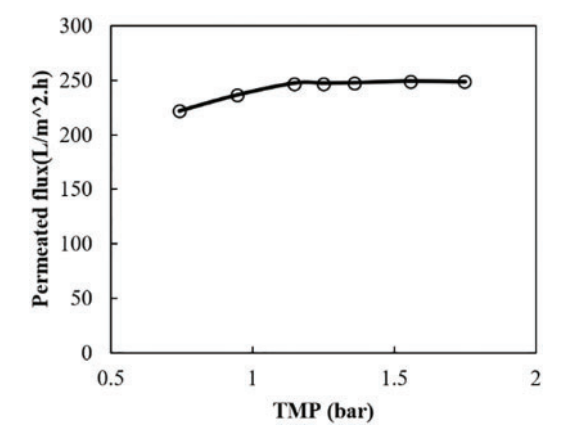


Fig. 6. TMP effect on purified water flux at 2.25 (m/s).

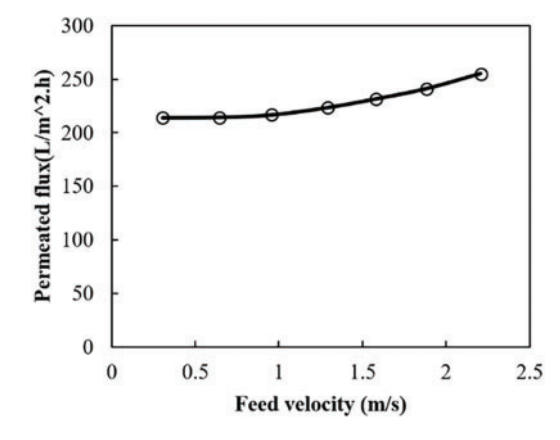


Fig. 7. Effect of the entrance velocity of feed on permeate flux.

In another investigation, the effect of feed velocity on the amount of permeate flux is measured. Theoretically, the increase in effluent velocity should reduce the thickness of the hydrodynamic boundary layer. That reduces the thickness of the layer resistant to mass transfer, ultimately leading to an increase in permeability. However, increasing the feed velocity will reduce the residence time inside the channel. The short residence time will decrease the component's opportunity to diffuse from the channel into the porous media, decreasing permeability flux. Determining which of these two opposing tendencies experimentally governs the system requires performing a sensitivity analysis with different feed velocities. Fig. 7

shows the performed sensitivity analysis and states that increasing the effluent velocity will increase the seepage flux due to the reason mentioned above.

#### 4. Conclusion

A multi-channel ceramic membrane is modeled with a realistic three-dimensional configuration containing 19 channels along with a porous medium. The effluent mass flux and inlet flow velocity of a lab-scale ceramic membrane designed to treat wastewater containing oily and greasy compounds are predicted. The model precisely showed the TMP effect in the porous medium. Additionally, the permeate mass flux variations are also demonstrated in different inlet velocities.

#### CONFLICT OF INTEREST

Authors declare that they do not have any conflict of interest.

#### REFERENCES

- Ahmed SF, Mehejabin F, Momtahin A, Tasannum N, Faria NT, Mofijur M, et al. Strategies to improve membrane performance in wastewater treatment. Chemosphere. 2022 Jun;30;306:135527. doi: 10.1016/j.chemosphere.2022.135527.
- Adam MR, Othman MH, Kurniawan TA, Puteh MH, Ismail AF, Khongnakorn W, et al. Advances in adsorptive membrane technology for water treatment and resource recovery applications: a critical review. J Environ Chem Eng. 2022 Jun 1;10(3):107633. doi: 10.1016/j.jece.2022.107633.
- Mohammed KI, Abdalla BK, Hago EE. Reverse osmosis options for water supply to a thermal power station. Eur J Eng Technol Res. 2019 Oct 26;4(10):143-6. doi: 10.24018/ejeng.2019.4.10.1506.
- Fazlifarda S, Allahgholia N, Mohammadia T, Bakhtiarib O. P84/ZIF-8 mixed matrix membranes for pervaporation dehydration of isopropanol. Desalin Water Treat. 2017 May 1;77:282-90. doi: 10.5004/dwt.2017.20886.
- Fazlifard S, Mohammadi T, Bakhtiari O. Chitosan/ZIF-8 mixed-matrix membranes for pervaporation dehydration of isopropanol. Chem Eng Technol. 2017 Apr;40(4):648-55. doi: 10.1002/ceat.201500499.
- Arzani M, Mahdavi HR, Sheikhi M, Mohammadi T, Bakhtiari O. Ceramic monolith as microfiltration membrane: preparation, characterization and performance evaluation. Appl Clay Sci. 2018 Sep 1;161:456–63. doi: 10.1016/j.clay.2018.05.021.
- [7] Chen X, Zhang Y, Tang J, Qiu M, Fu K, Fan Y. Novel pore size tuning method for the fabrication of ceramic multi-channel nanofiltration membrane. J Membr Sci. 2018 Apr 15;552:77-85. doi: 10.1016/j.memsci.2018.01.056.
- Cui Z, Xing W, Fan Y, Xu N. Pilot study on the ceramic membrane pre-treatment for seawater desalination with reverse osmosis in Tianjin Bohai Bay. *Desalination*. 2011 Sep 15;279(1–3):190–4. doi: 10.1016/j.desal.2011.06.008.
- Oliveira Neto GL, Oliveira NG, Delgado JM, Nascimento LP. Magalhães HL, Oliveira PL, et al. Hydrodynamic and performance evaluation of a porous ceramic membrane module used on the water-oil separation process: an investigation by CFD. Membr. 2021 Feb 8;11(2):121. doi: 10.3390/membranes11020121.
- [10] Frederic E, Guigui C, Jacob M, Machinal C, Krifi A, Line A, et al. Modelling of fluid flow distribution in multichannel ceramic membrane: application to the filtration of produced water. J Membr Sci. 2018 Dec 1;567:290–302. doi: 10.1016/j.memsci.2018.09.021.
- [11] Zare M, Ashtiani FZ, Fouladitajar A. CFD modeling and simulation of concentration polarization in microfiltration of oil-water emulsions; Application of an Eulerian multiphase model. Desalin. 2013 Sep 2;324:37-47. doi: 10.1016/j.desal.2013.05.022.
- [12] Tong Y, Huang L, Li W. CFD simulation of flow field and resistance in a 19-core tandem ceramic membrane module. Chin J Chem Eng. 2020;1;28(3):625-35. doi: 10.1016/j.cjche.2019.11.006.

[13] Abadi SR, Sebzari MR, Hemati M, Rekabdar F, Mohammadi T. Ceramic membrane performance in microfiltration of oily wastewater. Desalin. 2011 Jan;15;265(1-3):222-8. doi: 10.1016/j.desal.2010.07.055.